1 **The oomycete MAMP, arachidonic acid, and an *Ascophyllum nodosum*-derived plant**
2 **biostimulant induce defense metabolome remodeling in tomato**
3

4 Domonique C. Lewis[1], Timo van der Zwan[2*], Andrew Richards[2**], Holly Little[2], Gitta L. Coaker[1],
5 and Richard M. Bostock[1†]
6
7 [1]Department of Plant Pathology, University of California, Davis, CA 95616, USA
8 [2]Acadian Plant Health, Acadian Seaplants, Ltd., Dartmouth, Nova Scotia, Canada, B3B 1X8
9 [†]Corresponding author: R. M. Bostock; E-mail: rmbostock@ucdavis.edu
10
11 [*]Current address: Symvivo Corporation, Burnaby, BC, V5J 5J8, Canada
12 [**]Current address: Department of Plant Pathology, University of California, Davis, CA 95616,
13 USA
14
15
16 **Keywords:** elicitor, metabolomics, plant immunity, *Solanum lycopersicum*
17
18 **Funding:** Research supported in part by a Gates Millenium Scholars Program fellowship and
19 Jastro-Shields awards to DCL, and an unrestricted gift from Acadian Seaplants, LTD., to RMB.

20 **Abstract**

21 Arachidonic acid (AA) is an oomycete derived MAMP capable of eliciting robust defense
22 responses and inducing resistance in plants. Similarly, extract from the brown seaweed
23 *Ascophylum nodosum*, a plant biostimulant that contains AA, can also prime plants for defense
24 against pathogen challenge. A previous parallel study comparing the transcriptomes of AA and
25 ANE root-treated tomato demonstrated significant overlap in transcriptional profiles, a shared
26 induced resistance phenotype, and changes in accumulation of various defense-related
27 phytohormones. In this work, untargeted metabolomic analysis via LCMS was conducted to
28 investigate the local and systemic metabolome-wide remodeling events elicited by AA- and
29 ANE-root treatment in tomato. Our study demonstrated AA and ANE's capacity to locally and
30 systemically alter the metabolome of tomato with enrichment of chemical classes and
31 accumulation of metabolites associated with defense-related secondary metabolism. AA and
32 ANE root-treated plants showed enrichment of fatty acyl-glycosides and strong modulation of
33 hydroxycinnamic acids and derivatives. Identification of specific metabolites whose
34 accumulation was affected by AA and ANE treatment revealed shared metabolic changes
35 related to ligno-suberin biosynthesis and the synthesis of phenolic compounds. However, AA-
36 and ANE-induced metabolomes are distinct, and do not share the extensive overlap in their
37 induced transcriptomes that we observed in a previous study. This study highlights the
38 extensive local and systemic metabolic changes in tomato induced by treatment with a fatty
39 acid MAMP and a seaweed-derived plant biostimulant with implications for induced resistance
40 and crop improvement.

41

42 **Introduction**

43 Plants have pre-formed and inducible structural and biochemical mechanisms to prevent or
44 arrest pathogen ingress and colonization. These defenses include barriers such as papillae and
45 ligno-suberized layers to fortify cell walls, and low-molecular weight inhibitory chemicals
46 (Freeman and Beattie 2008). Plants undergo transcriptional changes upon perception of
47 microbe associated molecular patterns (MAMPs) or effectors to induce local and systemic
48 resistance.

49 The oomycete MAMPs, arachidonic acid (AA) and eicosapentaenoic acid (EPA), are
50 potent elicitors of defense. These eicosapolyenoic acids were first identified as active
51 components in *Phytophthora infestans* spore and mycelial extracts capable of eliciting a
52 hypersensitive-like response, phytoalexin accumulation, lignin deposition, and protection
53 against subsequent infection in potato tuber discs (Bostock et al. 1981; Bostock et al. 1982).
54 Further work demonstrated root treatment with AA protects tomato and pepper seedlings
55 from root and crown rot caused by *Phytophthora capsici*, with associated lignification at sites of
56 attempted infection (Dye and Bostock 2021). AA has been shown to induce resistance, elicit
57 production of reactive oxygen species, and trigger programmed cell death in members of the
58 Solanaceae and other families (Araceli et al. 2007; Bostock et al. 1981; Cook et al. 2018;
59 Dedyukhina et al. 2014; Dye et al. 2020; Knight et al. 2001).

60

61 Phaeophyta and Rhodophyta members (red and brown macroalgae) contain numerous
62 bioactive chemicals that can elicit defense responses in plants (Klarzynski et al. 2003; Sangha et
63 al. 2010; Vera et al. 2011). The brown alga, *Ascophyllum nodosum*, is a rich source of

64 polyunsaturated fatty acids, including AA and EPA, which comprise nearly 25% of its total fatty
65 acid composition (Lorenzo et al. 2017; van Ginneken et al. 2011). *A. nodosum* and oomycetes
66 belong to the major eukaryotic lineage, the Stramenopila, and share other biochemical features
67 (e.g., both are rich in β-1,3-glucans). Commercial extracts of *A. nodosum*, used in organic and
68 conventional agriculture as plant biostimulants, may also help plants cope with biotic and
69 abiotic stresses. A proprietary *A. nodosum* extract, Acadian (hereafter ANE; APH-1011-00,
70 Acadian Seaplants, Ltd., Nova Scotia, Canada), has been shown to provide protection against
71 bacterial and fungal pathogens (Ali et al. 2016a). Studies in *A. thaliana* showed ANE induced
72 systemic resistance to *Pseudomonas syringae* pv. *tomato* and *Sclerotinia sclerotiorum*
73 (Subramanian et al. 2011). Investigation into ANE-induced resistance in *A. thaliana* and tomato
74 suggest the role of ROS production, jasmonic acid signaling, and upregulation of defense-
75 related genes and metabolites (Ali et al. 2016b; Cook et al. 2018; Jayaraj et al. 2008;
76 Subramanian et al. 2011). As a predominant polyunsaturated fatty acid in ANE, AA may
77 contribute to ANE's biological activity.

78 In a parallel study we demonstrated AA's ability to systemically induce resistance and
79 ANE's capacity to locally and systemically induce resistance in tomato to different pathogens
80 (Lewis et al. 2022). Further, we showed that AA and ANE altered the phytohormone profile of
81 tomato by modulating the accumulation of defense-related phytohormones (Lewis et al. 2022).
82 Through RNA sequencing, this same study revealed a striking level of transcriptional overlap in
83 the gene expression profiles of AA- or ANE-root-treated tomato across tested timepoints (Lewis
84 et al. 2022). Gene ontology functional analysis of transcriptomic data revealed AA and ANE
85 enriched similar categories of genes with nearly perfect overlap also observed in categories of

86 under-represented genes. Both AA and ANE treatment protected seedings from challenge with
87 pathogens with different parasitic strategies while eliciting expression of genes involved in
88 immunity and secondary metabolism. The shared induced resistance phenotype and extensive
89 transcriptional overlap of AA and ANE treatments suggested similar metabolic changes may be
90 occurring in treated plants. In the current study, untargeted metabolomic analyses were
91 conducted to assess global effects of root treatment with AA and the AA-containing complex
92 extract, ANE, on the metabolome of tomato plants.
93

94 **Materials and Methods**

95

96 **Plant growth and root treatment**

97 ***Plant materials and hydroponic growth system***

98 Seeds of tomato (*Solanum lycopersicum cv.* 'New Yorker') were surface-sterilized and
99 germinated for 10 days on germination paper. Seedlings were transferred to a hydroponic
100 growth system and maintained in a growth chamber as previously described in (Dye et al.
101 2020). Seed was obtained from a commercial source (Totally Tomatoes, Randolph, WI).
102

103 ***Root treatment and tissue harvest***

104 Fatty acid sodium salts (Na-FA; Nu-Chek Prep, Elysian, MN) were prepared and stored as
105 previously described (Dye et al. 2020). A proprietary formulation of *A. nodosum* extract (ANE;
106 APH-1011-00; Acadian Seaplants, Ltd., Nova Scotia, Canada) was diluted with deionized water
107 (diH2O) to a 10% working concentration, which was used to prepare treatment dilutions. All

108 chemicals were diluted to their treatment concentrations with sterile diH_2O. Hydroponically
109 reared, 3-week-old tomato seedlings with two fully expanded true leaves were transferred to 1
110 L darkened treatment containers with their respective root treatment solutions. Following 24,
111 48, 72, and 96 hours of root treatment, tomato seedlings were removed from treatment
112 containers, and leaves and roots were excised from shoots and flash frozen in liquid nitrogen.
113 Each sample was the pool of roots or leaves of two seedlings with four replications per tissue,
114 treatment, and timepoint.
115
116 **Metabolite extraction**
117 Samples were transported on dry ice and stored at −70 °C until metabolite extraction. Tissue
118 samples were ground in liquid nitrogen using a mortar and pestle and 100 mg was weighed and
119 transferred to a 2-ml bead-beating tube containing four 2.8-mm ceramic beads. All tools and
120 consumables were pre-chilled in liquid nitrogen. After weighing, each sample was removed
121 from liquid nitrogen and kept at −20 °C until addition of extraction solution.
122 One ml of extraction solution (80 % v/v methanol and 0.1 % v/v formic acid in ultrapure water)
123 was added to each sample which was then vortexed, followed by bead-beating in a bead mill
124 (Bead Mill 24, Fisherbrand) at a speed of 2.9 m/s for one 3-min cycle. After bead-beating,
125 samples were centrifuged at 12k × *g* for 10 min at 4 °C (Accu Spin Micro 17R, Thermo Scientific).
126 Samples were diluted 5-fold using extraction solution and filtered into LCMS-grade HPLC vials
127 using 0.22-µm PTFE syringe filters. HPLC vials were kept at 4 °C until LCMS analysis. A blank was
128 prepared by adding 1 ml extraction solution to a bead-beating tube containing beads that was

129 processed equivalently to the samples. In addition, a quality control sample was prepared by
130 combining 20 µl of each of the extracted samples and processed equivalently.
131
132 **Liquid chromatography/mass spectrometry run conditions**
133 Samples were analyzed via high performance liquid chromatography (Agilent 1260 Infinity) and
134 electrospray ionization quadrupole time-of-flight mass spectrometry (Agilent 6530 Q-TOF)
135 controlled by MassHunter software in centroid data mode. Mobile phase A was ultrapure water
136 with 0.05 % (v/v) formic acid and mobile phase B was acetonitrile with 0.05 % (v/v) formic acid.
137 Before starting the run, the column (Poroshell 120 EC-C18; 3.0 mm internal diameter, 50 mm
138 length, 2.7 µm particle size; Agilent), equipped with a guard column (EC-C18; 3.0 mm internal
139 diameter, 5 mm length, 2.7 µm particle size; Agilent), was conditioned for 20 minutes with 95 %
140 mobile phase A and 5 % B. Column temperature was maintained at 40 °C. The sample injection
141 order was randomized, with individual samples being run consecutively in positive and negative
142 mode. The quality control sample was injected at the beginning and end of the run, as well as
143 after every 12 samples throughout the run to check signal and elution stability. Source
144 parameters were as follows: drying gas temperature of 325 °C (positive) and 350 °C (negative),
145 drying gas flow 12 l/min, nebulizer pressure 35 psi, sheath gas temp 375 °C (positive) and 400
146 °C (negative), sheath gas flow 11 l/min, capillary voltage 3500 V (positive) and 3000 V
147 (negative), nozzle voltage 0 V (positive) and 1500 V (negative), fragmentor 125 V, skimmer 65 V,
148 and octopole 750 V. Acquisition was performed over a mass range of 50 to 1700 m/z using the
149 all-ions MS/MS technique, cycling three different collision energies (0, 10, 30 eV) at an
150 acquisition rate of 3 spectra/s. Simultaneous infusion of a solution of purine and hexakis(1H,

151 1H, 3H-tetrafluoropropoxy)phosphazine using the reference nebulizer was used throughout the
152 runs for mass calibration. Samples were introduced using 2 µl injections at a flow rate of 0.5
153 ml/min. A needle wash of 1:1 acetonitrile:water was used between each injection. The mobile
154 phase gradient was: 0 min, 95 % A, 5 % B; 1 min, 95 % A, 5 % B; 10 min, 50 % A, 50 % B; 15 min,
155 0 % A, 100 % B; 17 min, 0 % A, 100 % B; 17.1 min, 95 % A, 5 % B; 19.1 min, 95 % A, 5 % B.
156

157 **Data analysis pipeline**

158

159 ***Data alignment, deconvolution, and normalization***

160 Positive and negative mode raw data files from MassHunter were analysed separately in MS-
161 DIAL (v. 4.80) before downstream analysis. Tolerances for MS1 and MS2 were set to 0.025 and
162 0.075 Da respectively (Tsugawa et al. 2015). A representative quality control sample run was
163 used as the reference file to align peaks. For peak detection, the mass slice width was set to 0.1
164 DA and the minimum peak height was set to 15,000 which was approximately 3 times the noise
165 level observed in the total ion chromatogram. A linear weighted moving average method was
166 used for peak smoothing, with a smoothing level of 3 scans and a minimum peak width of 5
167 scans. Deconvolution was performed with a sigma window value of 0.5 and an MS/MS
168 abundance cutoff of 10. The adducts permitted were $[M+H]+$, $[M+NH_4]+$, $[M+Na]+$, $[M+K]+$,
169 $[M+H-H_2O]+$, and $[2M+H]+$ in positive mode, and $[M-H]-$, $[M-H_2O-H]-$, $[M+Cl]-$, $[M+Na-2H]-$,
170 and $[M+K-2H]-$ in negative mode.

171

172 ***Quality control, feature annotation, and merging***

173 MS-DIAL data was cleaned in MS-CleanR (*mscleanr*, v. 1.0) in RStudio (v. 1.4.1106) using the
174 following parameters: minimum blank ratio of 0.8, maximum relative standard deviation of 30,
175 minimum relative mass defect (RMD) of 50, maximum RMD of 3000, maximum mass difference
176 of 0.05 and maximum retention time difference of 0.15. MS-DIAL features were clustered by
177 applying a Pearson correlation, with a minimum correlation of 0.8 and maximum p value of
178 0.05, retaining two features per cluster according to most intense and the most connected peak
179 filters (Fraisier-Vannier et al. 2020). Selected peaks were imported into MS-FINDER (v. 3.52) for
180 annotation (Tsugawa et al. 2016). Mass tolerance for MS1 and MS2 were set to 5 and 15 ppm
181 respectively, the relative abundance cut off set at 1% and the formula finder was configured to
182 use C, H, O, N, P, and S atoms. FooDB, PlantCyc, ChEBI, NPA, NANPDB, COCONUT, KNApSAcK,
183 PubChem, and UNPD were used as local databases. During the final merge step in MS-CleanR,
184 the best annotation for each peak was based on MS-FINDER scores. The normalized annotated
185 peaks list produced by MS-CleanR was used for the final statistical analyses in R.
186
187 ***Statistical analysis***
188 All statistical analyses were completed in R (v. 4.0.5) via RStudio (v. 1.4.1106). Statistical
189 analyses were run separately for each tissue type using the same parameters.
190
191 ***Multivariate analyses***
192 A partial least squares (PLS) supervised model of the complete log-transformed and Pareto-
193 scaled dataset was done using the *ropls* package (version 1.22.0), with the three treatment
194 groups as the response variables. Ellipses were drawn around treatments using *stat_ellipse*

195 (*ggplot2*) based on a 95 % confidence level. This distance type considers the correlation
196 between variables and the ellipses are created around the centroid data point.
197 Heatmaps were created using the log-transformed data within the *ComplexHeatmap* package in
198 R (v. 2.13.1), with hierarchical clustering according to the complete-linkage method and
199 Euclidean distance measure across columns and rows, displayed as dendrograms.
200

201 ***Pairwise multivariate analyses***

202 Pairwise multivariate analysis was performed across all time points between ANE and H_2O, and
203 between AA and H_2O, using an orthogonal projections to latent structures discriminant analysis
204 (OPLS-DA). OPLS-DA models were generated using the *ropls* package, with the predictive
205 components set to 1 and orthogonal components to 7. S-plots were generated following
206 sample sum normalization and Pareto scaling via calculation of p1 (covariance) and pcorr1
207 (correlation) of the OPLS-DA scores using the *muma* package (v. 1.4) source code within R.
208 Chemical class enrichment analysis was achieved using ChemRICH (version 1.0 August 2020) for
209 each two-treatment comparison at each time point within R using the source code (Barupal and
210 Fiehn 2017). A student's t-test of the signal was conducted to generate p values and effect size.
211 The effect size in each case represents the difference compared to the water control treatment
212 group.
213

214 **Results**

215 ***Local and systemic metabolomic analysis of AA- and ANE- induced plants***

216 Previous transcriptomic work revealed a high level of congruency in differentially expressed
217 genes in AA- and ANE-treated tomato seedlings compared to H_2O-treated controls (Lewis et al.
218 2022). To further this line of investigation, the metabolomic profiles of AA- and ANE-root-
219 treated plants were compared to H_2O after 24-, 48-, 72-, and 96-hours exposure to their
220 respective treatments. Locally-treated roots and distal leaves were harvested, flash frozen,
221 extracted for metabolites, and subsequently analyzed via liquid chromatography/mass
222 spectrometry (**Fig. 1A**).
223 Partial least squares (PLS) score plots of tomato root tissue revealed distinct clustering
224 by treatment irrespective of timepoint (**Fig. 1C**). No overlap was observed in the 95%
225 confidence ellipses for any treatment group. Likewise, heatmap visualization of the $\log_{10}$ signal
226 of metabolites showed clear clustering of metabolomic profiles by treatment (**Fig. 1B**).
227 Features displayed in the heatmap were filtered from the total dataset with a p-value $< 10^{-6}$ and
228 absolute fold change > 5 in roots.
229 Less defined clustering was observed in PLS score plots of distal leaf tissue across
230 sampled timepoints (**Fig. 2B**). Ellipses representing the 95% confidence interval for both H_2O
231 and AA treatments both partially overlap with the ANE treatment group. Similarly, a heatmap
232 depicting metabolite $\log_{10}$ signal showed more diffuse clustering by treatment (**Fig. 1A**).
233 Visualized metabolites from leaves displayed in the heatmap used a p-value < 0.001 and an
234 absolute fold-change > 2.
235
236 ***Chemical enrichment analysis of AA- and ANE-induced plants***

237 Chemical enrichment analyses were conducted to identify classes of metabolites whose
238 accumulation was locally or systemically altered in AA- and ANE-root-treated tomato seedlings.
239 Enrichment analyses of metabolites whose mean signal was significantly changed in AA- or
240 ANE-treated plants compared to H_2O identified numerous affected chemical classes **(Fig. 3 and**
241 **Sup. Fig. 1)**. These changes were most robust in directly treated roots compared to distal
242 leaves. Treatment of tomato seedlings with AA showed strong modulation of metabolomic
243 features classified as triterpenoids and linoleic acid and derivatives in roots. AA-treated roots
244 also showed increases in hydroxycinnamic acids and derivatives and fatty acyl glycosides of
245 mono- and disaccharides. ANE-treated roots showed modulation in the accumulation of
246 triterpenoids, steroidal glycosides, and hydroxycinnamic acids and derivatives. Similar to AA-
247 treated plants, the roots of plants treated with ANE also showed increases in metabolites
248 classified as fatty acyl glycosides of mono- and di-saccharides.
249 Although less striking than the chemical enrichment analysis of roots, leaf tissue of root-
250 treated plants did reveal an altered metabolome **(Sup. Fig. 1)**. These changes in metabolite
251 accumulation occurred most prominently at 96 hours, the latest tested timepoint. Increases in
252 sesquiterpenoids and steroidal saponins were seen in leaves of AA-treated plants at 96 hours.
253 A mix of accumulation and suppression of terpenoids and an increase of methoxyphenols was
254 observed in the leaves of ANE-root-treated plants.
255
256 ***Specific metabolomic features modulated by AA- and ANE- root treatments***
257 Chemical enrichment analyses broadly revealed classes of metabolites that were induced or
258 suppressed in AA- or ANE-treated plants. To examine which specific variables (metabolites)

259 provide the strongest discriminatory power between the two treatment groups, a two-group
260 comparative supervised multivariate analysis, orthogonal projections to latent structures
261 discriminant analysis (OPLS-DA), was utilized. OPLS-DA score plots show strong between-group
262 variability discrimination between AA and ANE treatment groups compared to the H_2O control
263 across all tested timepoints with the x-axis describing the inter-treatment variability, and the y-
264 axis showing the intra-treatment variability **(Suppl. Figure 2).** S-plots derived from OPLS-DA
265 were examined for both AA and ANE treatments in pairwise comparison with H_2O control. S-
266 plots of OPLS-DA revealed that treatment with AA or ANE induced shared changes in the levels
267 of several defense-related metabolites in roots **(Fig. 4)**. Variables (metabolites) with the most
268 negative and positive correlation and covariance values are the most influential in the model.
269 These metabolites are located on either tail of the S-plot (upper-right and lower-left) and
270 contribute most greatly to the separation between treatment groups
271 Bar charts depicting mean LCMS signals for top OPLS-DA S-plot metabolites visualized
272 across all timepoints illustrate that AA and ANE have similar effects on plant metabolic response
273 **(Fig. 5)**. Treatment of tomato roots with AA and ANE resulted in a sharp increase in metabolic
274 intermediates in ligno-suberin biosynthesis. This includes AA-induced accumulation of
275 moupinamide (syn. N-feruloyltyramine) and significant increases in coniferyl alcohol in the
276 roots of ANE-treated plants across all tested timepoints. In roots, AA and ANE treatments also
277 induced increased levels of N-(p-hydroxyphenyl)ethyl p-hydroxycinnamide and N1-trans-
278 feruloylagmatine compared to H_2O treatment, reflecting strong upregulation of the shikimate
279 pathway and phenolic compound synthesis. Reduced levels of tomatine and dehydrotomatine
280 were observed in the roots of AA- and ANE-treated plants indicating suppression of steroid

281 glycoalkaloid biosynthesis. Treated plants also showed lower levels of lyso-phosphatidyl
282 ethanolamine (0:0/18:2(9Z,12Z)) that could reflect enhanced membrane lipid turnover.
283

284 **Discussion**

285 AA and ANE can induce disease resistance locally and systemically, alter the accumulation of
286 key phytohormones, and change the transcriptional profile of tomato with a striking level of
287 overlap between the two treatments (Lewis et al. 2022). The current study examined and
288 characterized the AA- and ANE-induced metabolomes of tomato. AA and ANE locally and
289 systemically induce metabolome remodeling toward defense-associated metabolic features.
290 Early studies investigating transcriptional and metabolic changes in potato revealed
291 selective partitioning and shifting of terpenoid biosynthesis from steroidal glycoalkaloids to
292 sesquiterpenes following treatment with AA or EPA or challenged with *P. infestans* (Choi et al.
293 1992; Stermer and Bostock 1987; Tjamos and Kuc 1982). Similarly, our work here with AA- and
294 ANE-treated tomato seedlings has shown a marked decrease in the levels of two abundant
295 glycoalkaloids, tomatine and dehydrotomatine **(Fig. 5)**. Our data also show strong enrichment
296 of sesquiterpenes in leaves of AA-treated plants at 96 hours post treatment, although the
297 identity of these sesquiterpenes is unresolved **(Sup. Fig. 1A)**. This work further supports
298 evidence for differential regulation and sub-functionalization of sterol/glycoalkaloid and
299 sesquiterpene biosynthetic pathways in solanaceous plants in different stress contexts (Choi et
300 al. 1992; Stermer and Bostock 1987).
301 AA and EPA are strong elicitors that are abundant in structural and storage lipids of
302 oomycete pathogens, but absent from higher plants. Although their initial perception by the

303 plant is likely different from that of canonical MAMPs (e.g., flg22, chitosan, lipopolysaccharide),
304 there is some convergence in downstream defenses induced by these various MAMPs. Work to
305 characterize the effect of canonical MAMP treatment on the metabolomes of various plant
306 species has implicated common metabolic changes that prime for defense. Cells and leaf tissue
307 of *A. thaliana* treated with lipopolysaccharide (LPS) showed enrichment of phenylpropanoid
308 pathway metabolites, including cinnamic acid derivatives and glycosides (Finnegan et al. 2016).
309 In the same study, SA and JA were also positively correlated with LPS treatment, as we also
310 observed in tomato following treatment with AA (Finnegan et al. 2016; Lewis et al. 2022).
311 Recent work in *A. thaliana* wild-type and receptor mutants treated with two chemotypes of LPS
312 showed increases in hydroxycinnamic acid and derivatives and enrichment of the associated
313 phenylpropanoid pathway (Offor et al. 2022). Work in tobacco similarly found treatment with
314 LPS, chitosan, and flg22 all induced accumulation of hydroxycinnamic acid and derivatives, and
315 that defense responses elicited by these MAMPs were modulated by both SA and JA (Mhlongo
316 et al. 2016). More recent work in the cells of *Sorghum bicolor* treated with LPS showed
317 enrichment of hydroxycinnamic acids and other phenylpropanoids in coordination with
318 accumulation of both SA and JA (Mareya et al. 2020). Treatment of tomato with flg22 and flgII-
319 28 also enriched hydroxycinnamic acids, and tomato treatment with cps22 revealed a
320 metabolic shift toward the phenylpropanoid pathway with hydroxycinnamic acid, conjugates
321 and derivatives as key biomarkers (Zeiss et al. 2021a, b). Similar to traditional MAMPs, AA and
322 the AA/EPA-containing complex mixture, ANE, both induce enrichment of cinnamic acid and
323 derivatives in tomato seedlings **(Fig. 3)**. This supports the hypothesis that MAMPs broadly

324 induce similar metabolic changes to enrich pools of specialized secondary metabolites that
325 contribute to plant immunity.

326 AA- and ANE-treated roots showed strong enrichment of metabolic features classified as
327 fatty acyl glycosides of mono- and disaccharides **(Fig. 3)**. Fatty acyl glycosides have been
328 studied in several plant families and are most extensively characterized in members of
329 Solanaceae (Asai and Fujimoto 2010; Asai et al. 2010; Dalsgaard et al. 2006; Moghe et al.
330 2017). Investigations into the function of fatty acyl glycosides in plants suggest they may act to
331 protect against insect herbivory through various mechanisms and provide protection against
332 fungal pathogens (Leckie et al. 2016; Luu et al. 2017; Puterka et al. 2003; Simmons et al. 2004;
333 Weinhold and Baldwin 2011). A recent study isolated and identified fatty acyl glycosides from
334 strawberry capable of inducing immune responses in *A. thaliana*, including ROS burst, callose
335 deposition, increased expression of defense-related genes, and induced resistance to bacterial
336 and fungal challenge (Grellet Bournonville et al. 2020). This same work also demonstrated that
337 the strawberry-derived fatty acyl glycosides induced resistance in soybean and, due to their
338 antimicrobial activity, also protected lemon fruits postharvest from fungal infection (Grellet
339 Bournonville et al. 2020). AA- and ANE-root treatments locally elicit accumulation of the same
340 class of defense associated metabolites that Grellet et al. illustrated to have direct antimicrobial
341 activity and protect against disease (Grellet Bournonville et al. 2020).

342 Cell wall fortification is an important plant defense often initiated upon pathogen
343 infection. Cell wall lignification is a well-studied mechanism with localized accumulation of
344 phenolic intermediates and lignin at attempted penetration sites (Nicholson and
345 Hammerschmidt 1992; Vance et al. 1980; Zeyen et al. 2002). Lignification reinforces and

346 rigidifies the cell wall to create an impervious barrier to microbial ingress (Nicholson and
347 Hammerschmidt 1992; Vance et al. 1980; Zeyen et al. 2002). In our study, AA treatment of
348 tomato roots induced accumulation of a phenylcoumaran intermediate in lignin biosynthesis,
349 while ANE treatment induced accumulation of coniferyl alcohol, an important monomer unit of
350 lignin. Interestingly, coniferyl alcohol has recently been shown to act in a signaling capacity in a
351 regulatory feedback mechanism to intricately control lignin biosynthesis, an irreversible process
352 that is energetically costly (Guan et al. 2022). The findings of our study coincide with the well-
353 characterized role of lignin and its intermediates in plant defense.

354 Despite similarity in changes to the metabolic profile of tomato, the degree of
355 transcriptional overlap previously identified in AA- and ANE-treated plants is not reflected in
356 the degree of metabolic overlap here. Principle component analysis showed AA and ANE
357 transcriptomes clustered tightly together, while metabolomic data indicate discreet clustering
358 of AA and ANE treatments (Lewis et al. 2022). This suggests that although largely overlapping
359 changes to gene expression occur, more varied and distinctive metabolic outcomes can result.

360 This work characterizes local and systemic metabolic profiles of AA- and ANE-treated
361 tomato with the oomycete-derived MAMP, AA, and the AA-containing biostimulant, ANE. AA
362 and ANE profoundly alter the tomato metabolome toward defense-associated secondary
363 metabolites with notable overlap in enriched metabolite classes compared to H_2O control.
364 Further investigation is required to elucidate the functional contribution of these metabolic
365 features in AA- and ANE induced resistance and, more broadly, plant immunity. Our study adds
366 to the understanding of MAMP-induced metabolomes with implications for further
367 development of seaweed-derived biostimulants for crop improvement.

368

369 **Author contributions**

370 Study planned by all authors. Experiments performed by DCL, metabolite analyses conducted
371 by TVDZ and AR. Paper written by DCL and RMB, with editing by GLC.

372 **Literature cited**

373 Ali, N., Farrell, A., Ramsubhag, A., and Jayaraman, J. 2016a. The effect of *Ascophyllum nodosum* extract
374 on the growth, yield and fruit quality of tomato grown under tropical conditions. J. Appl. Phycol.
375 28:1353-1362.

376 Ali, N., Ramkissoon, A., Ramsubhag, A., and Jayaraj, J. 2016b. *Ascophyllum* extract application causes
377 reduction of disease levels in field tomatoes grown in a tropical environment. Crop Protect.
378 83:67-75.

379 Araceli, A.-C., Elda, C.-M., Edmundo, L.-G., and Ernesto, G.-P. 2007. Capsidiol production in pepper fruits
380 (*Capsicum annuum L.*) induced by arachidonic acid is dependent of an oxidative burst. Physiol.
381 Mol. Plant Pathol. 70:69-76.

382 Asai, T., and Fujimoto, Y. 2010. Cyclic fatty acyl glycosides in the glandular trichome exudate of *Silene*
383 *gallica*. Phytochemistry 71:1410-1417.

384 Asai, T., Hara, N., and Fujimoto, Y. 2010. Fatty acid derivatives and dammarane triterpenes from the
385 glandular trichome exudates of *Ibicella lutea* and *Proboscidea louisiana*. Phytochemistry 71:877-
386 894.

387 Barupal, D. K., and Fiehn, O. 2017. Chemical Similarity Enrichment Analysis (ChemRICH) as alternative to
388 biochemical pathway mapping for metabolomic datasets. Sci. Rep. 7:14567.

389 Bostock, R. M., Kuc, J. A., and Laine, R. A. 1981. Eicosapentaenoic and arachidonic acids from
390 *Phytophthora infestans* elicit fungitoxic sesquiterpenes in the potato. Science 212:67-69.

391 Bostock, R. M., Laine, R. A., and Kuć, J. A. 1982. Factors affecting the elicitation of sesquiterpenoid
392 phytoalexin accumulation by eicosapentaenoic and arachidonic acids in potato. Plant Physiol.
393 70:1417-1424.
394 Choi, D., Ward, B. L., and Bostock, R. M. 1992. Differential induction and suppression of potato 3-
395 hydroxy-3-methylglutaryl coenzyme A reductase genes in response to *Phytophthora infestans*
396 and to its elicitor arachidonic acid. Plant Cell 4:1333-1344.
397 Cook, J., Zhang, J., Norrie, J., Blal, B., and Cheng, Z. 2018. Seaweed extract (Stella Maris(®)) activates
398 innate immune responses in *Arabidopsis thaliana* and protects host against bacterial pathogens.
399 Mar. Drugs 16:221.
400 Dalsgaard, P. W., Potterat, O., Dieterle, F., Paululat, T., Kühn, T., and Hamburger, M. 2006. Noniosides E -
401 H, new trisaccharide fatty acid esters from the fruit of *Morinda citrifolia* (Noni). Planta Med.
402 72:1322-1327.
403 Dedyukhina, E. G., Kamzolova, S. V., and Vainshtein, M. B. 2014. Arachidonic acid as an elicitor of the
404 plant defense response to phytopathogens. Chem. Biol. Technol. 1:18.
405 Dye, S. M., and Bostock, R. M. 2021. Eicosapolyenoic fatty acids induce defense responses and
406 resistance to *Phytophthora capsici* in tomato and pepper. Physiol. Mol. Plant Pathol.
407 114:101642.
408 Dye, S. M., Yang, J., and Bostock, R. M. 2020. Eicosapolyenoic fatty acids alter oxylipin gene expression
409 and fatty acid hydroperoxide profiles in tomato and pepper roots. Physiol. Mol. Plant Pathol.
410 109:101444.
411 Finnegan, T., Steenkamp, P. A., Piater, L. A., and Dubery, I. A. 2016. The lipopolysaccharide-induced
412 metabolome signature in *Arabidopsis thaliana* reveals dynamic reprogramming of phytoalexin
413 and phytoanticipin pathways. PLoS One 11:e0163572.

414 Fraisier-Vannier, O., Chervin, J., Cabanac, G., Puech, V., Fournier, S., Durand, V., Amiel, A., André, O.,
415 Benamar, O. A., Dumas, B., Tsugawa, H., and Marti, G. 2020. MS-CleanR: A feature-filtering
416 workflow for untargeted LC–MS based metabolomics. Anal. Chem. 92:9971-9981.
417 Freeman, B., and Beattie, G. 2008. An overview of plant defenses against pathogens and herbivores.
418 Plant Health Instr. 149.
419 Grellet Bournonville, C., Filippone, M. P., Di Peto, P. d. l. Á., Trejo, M. F., Couto, A. S., Mamaní de
420 Marchese, A., Díaz Ricci, J. C., Welin, B., and Castagnaro, A. P. 2020. Strawberry fatty acyl
421 glycosides enhance disease protection, have antibiotic activity and stimulate plant growth. Sci.
422 Rep. 10:8196.
423 Guan, M., Li, C., Shan, X., Chen, F., Wang, S., Dixon, R. A., and Zhao, Q. 2022. Dual mechanisms of
424 coniferyl alcohol in phenylpropanoid pathway regulation. Front. Plant Sci. 13.
425 Jayaraj, J., Wan, A., Rahman, M., and Punja, Z. K. 2008. Seaweed extract reduces foliar fungal diseases
426 on carrot. Crop Protect. 27:1360-1366.
427 Klarzynski, O., Descamps, V., Plesse, B., Yvin, J.-C., Kloareg, B., and Fritig, B. 2003. Sulfated fucan
428 oligosaccharides elicit defense responses in tobacco and local and systemic resistance against
429 Tobacco Mosaic Virus. Mol. Plant-Microbe Interact. 16:115-122.
430 Knight, V. I., Wang, H., Lincoln, J. E., Lulai, E. C., Gilchrist, D. G., and Bostock, R. M. 2001. Hydroperoxides
431 of fatty acids induce programmed cell death in tomato protoplasts. Physiol. Mol. Plant Pathol.
432 59:277-286.
433 Leckie, B. M., D'Ambrosio, D. A., Chappell, T. M., Halitschke, R., De Jong, D. M., Kessler, A., Kennedy, G.
434 G., and Mutschler, M. A. 2016. Differential and synergistic functionality of acylsugars in
435 suppressing oviposition by insect herbivores. PLoS One 11:e0153345.

436 Lewis, D. C., Stevens, D. M., Little, H., Coaker, G. L., and Bostock, R. M. 2022. Overlapping local and
437 systemic defense induced by an oomycete fatty acid MAMP and brown seaweed extract in
438 tomato.2022.2008.2026.505481.
439 Lorenzo, J. M., Agregán, R., Munekata, P. E. S., Franco, D., Carballo, J., Şahin, S., Lacomba, R., and Barba,
440 F. J. 2017. Proximate composition and nutritional value of three macroalgae: *Ascophyllum*
441 *nodosum*, *Fucus vesiculosus* and *Bifurcaria bifurcata*. Mar. Drugs 15:360.
442 Luu, V. T., Weinhold, A., Ullah, C., Dressel, S., Schoettner, M., Gase, K., Gaquerel, E., Xu, S., and Baldwin,
443 I. T. 2017. O-acyl sugars protect a wild tobacco from both native fungal pathogens and a
444 specialist herbivore. Plant Physiol. 174:370-386.
445 Mareya, C. R., Tugizimana, F., Di Lorenzo, F., Silipo, A., Piater, L. A., Molinaro, A., and Dubery, I. A. 2020.
446 Adaptive defence-related changes in the metabolome of *Sorghum bicolor* cells in response to
447 lipopolysaccharides of the pathogen *Burkholderia andropogonis*. Sci. Rep. 10:7626.
448 Mhlongo, M. I., Piater, L. A., Madala, N. E., Steenkamp, P. A., and Dubery, I. A. 2016. Phenylpropanoid
449 defences in *Nicotiana tabacum* cells: overlapping metabolomes indicate common aspects to
450 priming responses induced by lipopolysaccharides, chitosan and flagellin-22. PLoS One
451 11:e0151350.
452 Moghe, G. D., Leong, B. J., Hurney, S. M., Daniel Jones, A., and Last, R. L. 2017. Evolutionary routes to
453 biochemical innovation revealed by integrative analysis of a plant-defense related specialized
454 metabolic pathway. ELife 6.
455 Nicholson, R. L., and Hammerschmidt, R. 1992. Phenolic compounds and their role in disease resistance.
456 Annu. Rev. Phytopathol. 30:369-389.
457 Offor, B. C., Mhlongo, M. I., Steenkamp, P. A., Dubery, I. A., and Piater, L. A. 2022. Untargeted
458 metabolomics profiling of Arabidopsis WT, *lbr-2-2* and *bak1-4* mutants following treatment with
459 two LPS chemotypes. Metabolites 12.

460 Puterka, G. J., Farone, W., Palmer, T., and Barrington, A. 2003. Structure-function relationships affecting
461 the insecticidal and miticidal activity of sugar esters. J. Econ. Entomol. 96:636-644.
462 Sangha, J. S., Ravichandran, S., Prithiviraj, K., Critchley, A. T., and Prithiviraj, B. 2010. Sulfated macroalgal
463 polysaccharides λ-carrageenan and ι-carrageenan differentially alter *Arabidopsis thaliana*
464 resistance to *Sclerotinia sclerotiorum* Physiol. Mol. Plant Pathol. 75:38-45.
465 Simmons, A. T., Gurr, G. M., McGrath, D., Martin, P. M., and Nicol, H. I. 2004. Entrapment of *Helicoverpa*
466 *armigera* (Hübner) (Lepidoptera: Noctuidae) on glandular trichomes of *Lycopersicon* species.
467 43:196-200.
468 Stermer, B. A., and Bostock, R. M. 1987. Involvement of 3-hydroxy-3-methylglutaryl coenzyme a
469 reductase in the regulation of sesquiterpenoid phytoalexin synthesis in potato. Plant Physiol.
470 84:404-408.
471 Subramanian, S., Sangha, J. S., Gray, B. A., Singh, R. P., Hiltz, D., Critchley, A. T., and Prithiviraj, B. 2011.
472 Extracts of the marine brown macroalga, *Ascophyllum nodosum*, induce jasmonic acid
473 dependent systemic resistance in *Arabidopsis thaliana* against *Pseudomonas syringae pv.*
474 *tomato* DC3000 and *Sclerotinia sclerotiorum*. Eur. J. Plant Pathol. 131:237-248.
475 Tjamos, E. C., and Kuc, J. A. 1982. Inhibition of steroid glycoalkaloid accumulation by arachidonic and
476 eicosapentaenoic acids in potato. Science 217:542-544.
477 Tsugawa, H., Kind, T., Nakabayashi, R., Yukihira, D., Tanaka, W., Cajka, T., Saito, K., Fiehn, O., and Arita,
478 M. 2016. Hydrogen rearrangement rules: computational MS/MS fragmentation and structure
479 elucidation using MS-FINDER software. Anal. Chem. 88:7946-7958.
480 Tsugawa, H., Cajka, T., Kind, T., Ma, Y., Higgins, B., Ikeda, K., Kanazawa, M., VanderGheynst, J., Fiehn, O.,
481 and Arita, M. 2015. MS-DIAL: data-independent MS/MS deconvolution for comprehensive
482 metabolome analysis. Nat. Methods 12:523-526.

483 van Ginneken, V. J., Helsper, J. P., de Visser, W., van Keulen, H., and Brandenburg, W. A. 2011.
484 Polyunsaturated fatty acids in various macroalgal species from North Atlantic and tropical seas.
485 Lipids Health Dis 10:104.
486 Vance, C., Kirk, T., and Sherwood, R. 1980. Lignification as a mechanism of disease resistance. Annu. Rev.
487 Phytopathol. 18:259-288.
488 Vera, J., Castro, J., Gonzalez, A., and Moenne, A. 2011. Seaweed polysaccharides and derived
489 oligosaccharides stimulate defense responses and protection against pathogens in plants. Mar.
490 Drugs 9:2514-2525.
491 Weinhold, A., and Baldwin, I. T. 2011. Trichome-derived O-acyl sugars are a first meal for caterpillars
492 that tags them for predation. PNAS 108:7855-7859.
493 Zeiss, D. R., Steenkamp, P. A., Piater, L. A., and Dubery, I. A. 2021a. Altered metabolomic states elicited
494 by Flg22 and FlgII-28 in *Solanum lycopersicum*: intracellular perturbations and metabolite
495 defenses. BMC Plant Biol. 21:429.
496 Zeiss, D. R., Steenkamp, P. A., Piater, L. A., and Dubery, I. A. 2021b. Metabolomic Evaluation of *Ralstonia*
497 *solanacearum* Cold Shock Protein Peptide (csp22)-Induced Responses in *Solanum lycopersicum*.
498 Front. Plant Sci. 12:803104.
499 Zeyen, R., Carver, T., and Lyngkjaer, M. 2002. Epidermal cell papillae In: Belanger R R, Bushnell WR (ed)
500 The powdery mildew: a comprehensive treatise. APS Press, MN, USA.

501

502

503

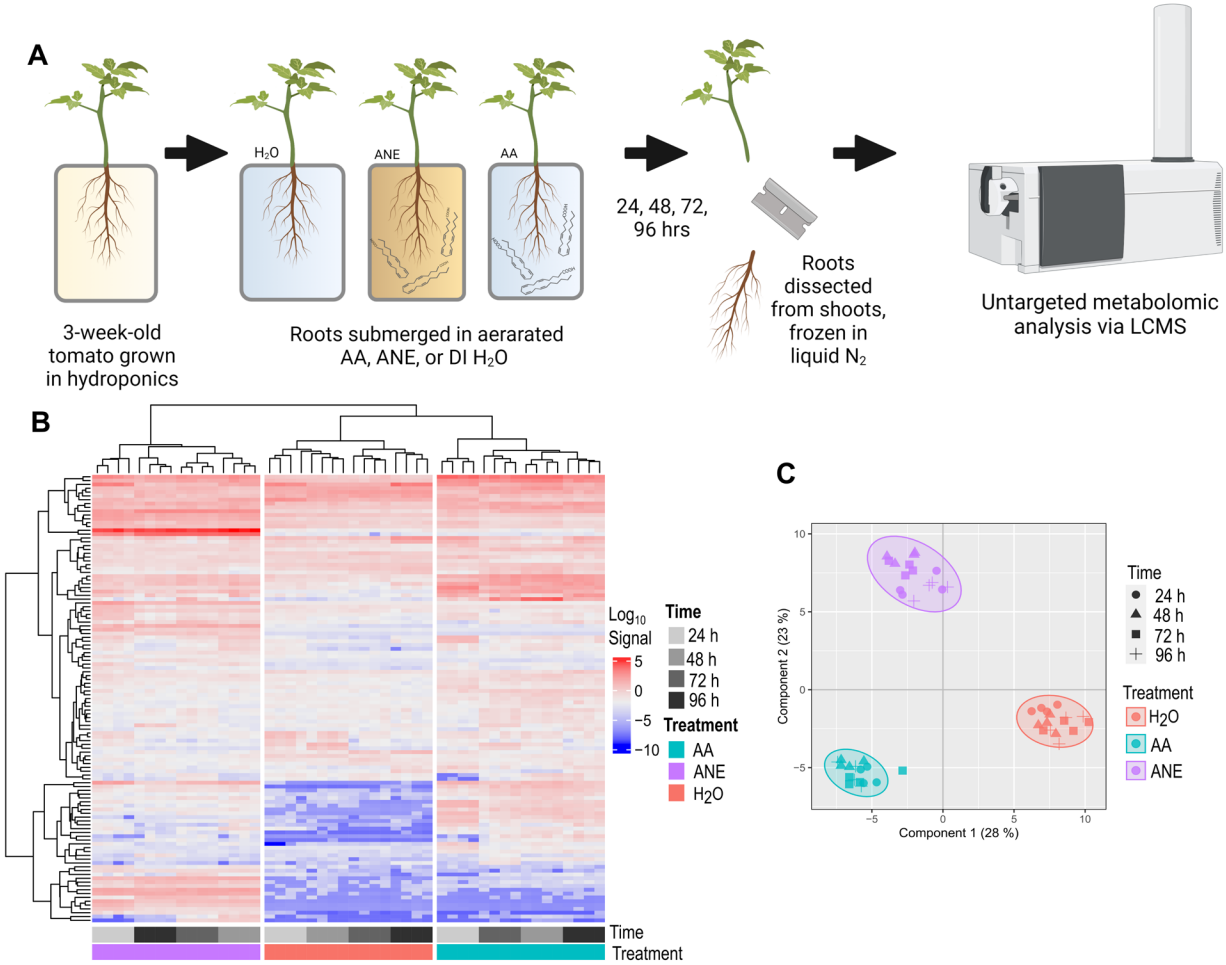

Figure 1. (A) Experimental procedure for the untargeted metabolomics study. Tomato roots were treated with 10 µM AA, 0.4% ANE, or H_2O. Following 24, 48, 72, and 96 hours of root exposure to their respective treatments, plants were harvested, root and leaf tissue dissected from shoots, and the collected tissue flash frozen in liquid nitrogen. Harvested tissue was then subjected to metabolite extraction and liquid chromatography/mass spectrometry. **(B)** Log10 signal of metabolites from root tissue of 10 µM AA-, 0.4% ANE-, or H_2O-treated plants sampled at 24, 48, 72, and 96 hours or treatment. Features visualized in the heatmap are filtered from the total dataset having an adjusted p-value < 10^{-6} and a fold change > 5. Heatmap data is log10 transformed and hierarchical clustering was conducted across rows and columns. **(C)**

514 Partial least squares score plots of tomato root metabolites after 24, 48, 72, and 96 hours of
515 treatment with 10 µM AA, 0.4% ANE, or H_2O. Ellipses indicate the 95% confidence intervals.
516 Score plots show variance of 4 biological replicates performed per timepoint and treatment.
517
518
519
520
521
522
523
524
525
526
527
528
529

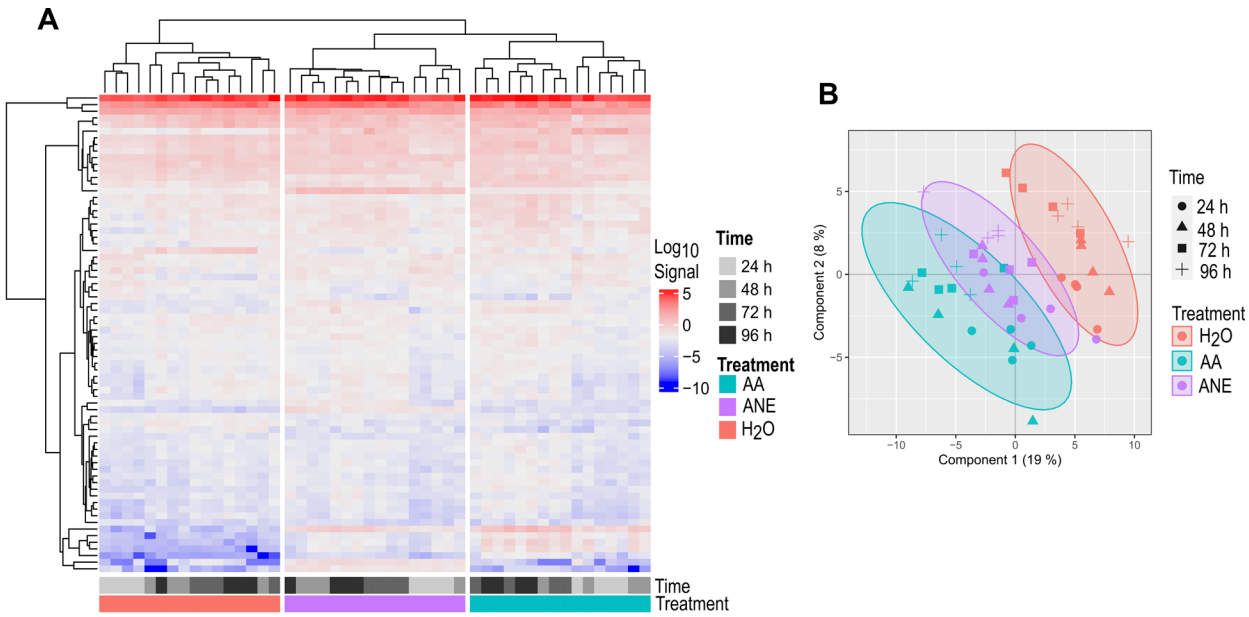

530

531 **Figure 2. (A)** Log10 signal of metabolites from leaf tissue of 10 µM AA-, 0.4% ANE-, or H_2O-

532 treated plants at 24, 48, 72, and 96 hours of treatment. Features visualized in the heatmap are

533 filtered from the total dataset having an adjusted p-value < 0.001 and a fold change > 2.

534 Heatmap data is log10 transformed and heirachical clustering was conducted across rows and

535 columns. **(B)** Partial least squares score plots of tomato leaf metabolites after 24,48, 72, and

536 96 hours of treatment with 10 µM AA, 0.4% ANE, or H_2O. Score plots show variance of 4

537 biological replicates performed per timepoint and treatment. Ellipses indicate the 95%

538 confidence intervals.

539

540

541

542

543

544

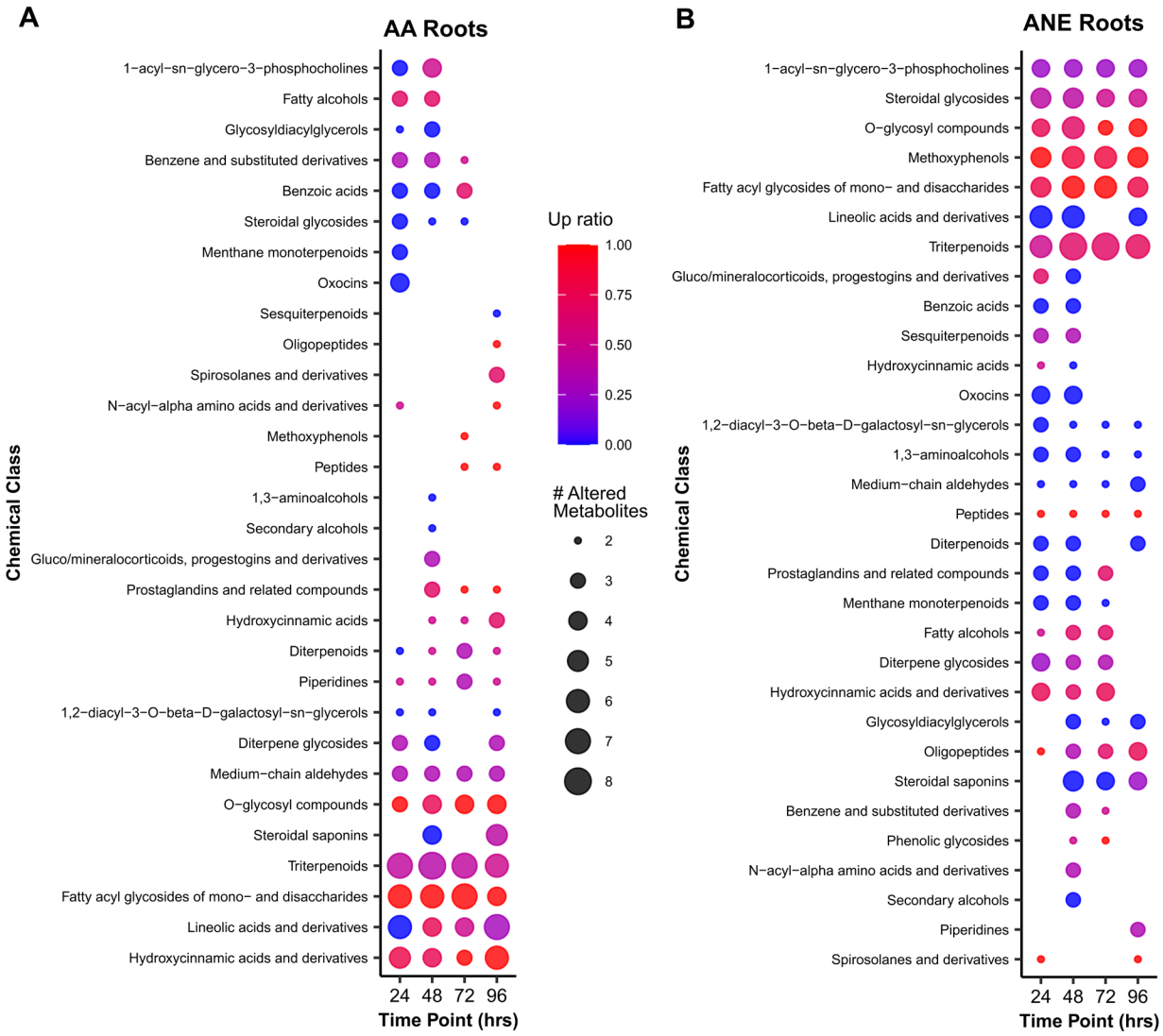

Figure 3. Dot plot illustrating chemical enrichment analysis of significantly altered metabolite clusters in roots of **(A)** AA- and **(B)** ANE-root-treated plants compared to H_2O after 24, 48, 72, 96 hours of treatment. Dot sizes indicate the number of altered metabolites per identified cluster. Dot color scale indicates the ratio of up (red) and down (blue) compounds in AA- and ANE-treated plants compared to H_2O. Up ratio represents the proportion of increased/decreased metabolites compared to H_2O.

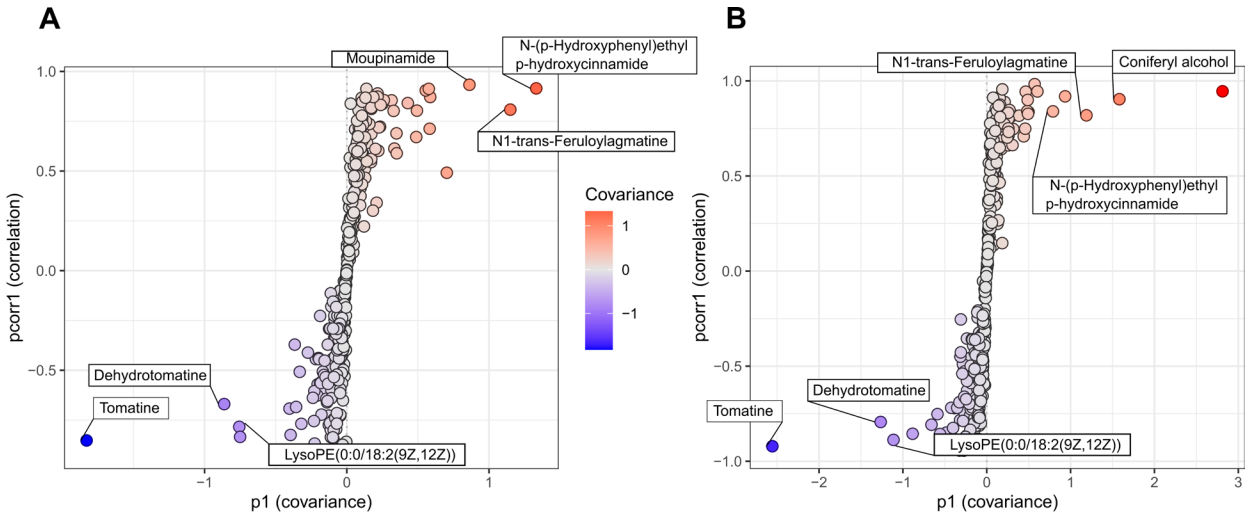

553

554 **Figure 4.** S-plots derived from orthogonal projections to latent structures discriminant analysis

555 (O-PLS-DA) models for the roots of **(A)** AA-treated and **(B)** ANE-treated plants in pairwise

556 comparison with H_2O across all tested timepoints. Color scale represents covariance strength

557 and direction with red data points indicating most positive covariance and blue indicating most

558 negative covariance.

559

560

561

562

563

564

565

566

567

568

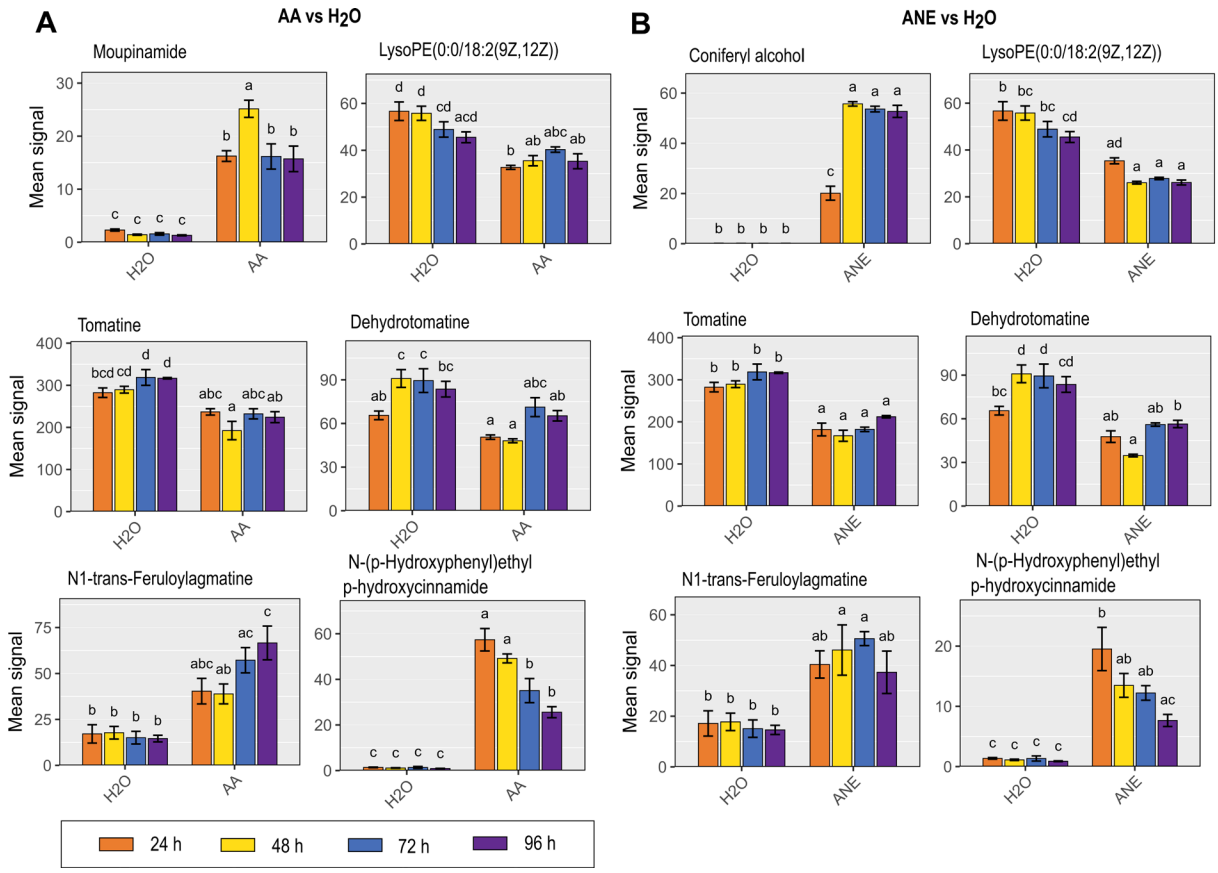

Figure 5. Mean LCMS signals for the top O-PLS-DA S-plot metabolites visualized across 24, 48, 72, and 96 hour timepoints for **(A)** AA- and **(B)** ANE-treated roots in pairwise comparison with H_2O.